Supplement of Atmos. Chem. Phys., 23, 14735–14760, 2023
https://doi.org/10.5194/acp-23-14735-2023-supplement

Atmospheric Chemistry and Physics
Open Access
EGU

Supplement of

Development, intercomparison, and evaluation of an improved mechanism for the oxidation of dimethyl sulfide in the UKCA model

Ben A. Cala et al.

Correspondence to: Ben A. Cala (ben.cala@nioz.nl) and Alexander T. Archibald (ata27@cam.ac.uk)

S1 Box model data

S1.1 BOXMOX input files

Table S1: Initial conditions in the box and background air

Species	Mixing ratio (ppm)
M	1.00E+06
N_2	7.80E+05
O_2	2.10E+05
H_2O	1.00E+04
CH_4	1.80E+00
CO	1.00E-01
H_2	5.00E-01
O_3	3.00E-02
H_2O_2	1.00E-03
NO	1.00E-06
NO_2	1.00E-05
HNO_3	5.00E-04
DMS	2.00E-04
SO_2	2.00E-05

Table S2: Diurnal profile of temperature and boundary layer height

Time (h)	Temperature (K)	Boundary Layer Height (m)
0	289.5359	1300
1	289.1363	1300
2	289.0000	1350
3	289.1363	1400
4	289.5359	1450
5	290.1716	1500
6	291.0000	1550
7	291.9647	1450
8	293.0000	1400
9	294.0353	1350
10	295.0000	1300
11	295.8284	1250
12	296.4641	1200
13	296.8637	1200
14	297.0000	1200

15	296.8637	1200
16	296.4641	1150
17	295.8284	1150
18	295.0000	1100
19	294.0353	1200
20	293.0000	1300
21	291.9647	1400
22	291.0000	1400
23	290.1716	1350
24	289.5359	1300

S1.2 Updating the standard DMS chemistry in CRIStrat 2

The H-abstraction pathway (reaction 1a,b) generates MTMP which is then further oxidised to SO_2 or CH_3SO_2 (reactions 2-7). The OH-addition pathway (reaction 1c) leads to dimethyl sulfoxide (DMSO, $(CH_3)_2SO$) and methanesulfinic acid (MSIA, $CH_3S(O)OH$) (reactions 8,9) and further oxidation through to CH_3SO_2 (reactions 10-12). Both pathways and the changes made are summarised in **Table 2**. The newly added reactions and their respective rate constants are largely based on Atkinson et al. (2004), the MCMv3.3.1 (Jenkin et al. 2015), and the primary literature therein.

The oxidation of MTMP by HO_2 (reaction 2c) was not previously included in the CS2 mechanism, but is expected to play a significant role at the low NO_x conditions over the remote ocean. Based on other $RO_2 + HO_2$ reactions, CH_3SCH_2OOH is the expected product, which has been detected through mass spectroscopy (Butkovskaya and LeBras, 1994). Since no experimental measurements exist for the kinetics of this reaction, the rate constant provided in the MCM was used. It is based on a generic expression, defined on the basis of available room temperature and temperature dependent data for alkyl and β-hydroxy RO_2 and it is dependent on the number of carbon atoms. Further oxidation of CH_3SCH_2OOH leads to the formation of methylthiolformate (MTF, CH_3SCHO) (reaction 3), a species that has been detected in chamber studies before under low NO_x conditions (Arsene et al., 1999, Urbanski et al., 1998). MTF decomposes to CH_3S (reaction 4), an intermediate that is already part of the CS2 DMS scheme as a reaction product of MTMP (reaction 2a,b).

CH_3S can add an O_2 to form a weakly bound adduct, CH_3SOO (reaction 5c). At 298 K at sea level, approximately one-third of CH_3S is present as the CH_3SOO adduct and at colder temperatures this ratio is even greater (75% at 273 K) (Turnipseed et al., 1992). CH_3SOO can decompose to CH_3 and SO_2 (reaction 6a), which proceeds through isomerization to CH_3SO_2, followed by rapid thermal decomposition (McKee, 1993, Butkovskaya and Barnes, 2002, Chen et al. 2021). Previous modelling studies, such as Hoffmann et al. (2016), include the isomerization step forming CH_3SO_2 but omit the decomposition. This could lead to a higher yield of MSA in those studies.

CH_3S can also be oxidised by O_3 and NO_2 to CH_3SO (reaction 5a,b). Measurements by Borissenko et al. (2003) show that O_3 oxidation of CH_3SO results in a 100% yield of SO_2 at pressures over 500 Torr (0.6 bar). Since the pressure in the marine boundary layer where most of DMS oxidation takes place is above this threshold, the products of reaction 7c_old were updated accordingly (reaction 7c). Additionally, the branching ratios of CH_3SO oxidation by NO_2 to CH_3SO_2 and SO_2 were revised to also match the findings by Borissenko et al. (2003).

While some CH_3SO_2 stems from the NO_3 oxidation of CH_3SO, it is mainly formed through oxidation of MSIA (reaction 9a,c), especially under low NO_x conditions. CH_3SO_2 can decompose to SO_2 (reaction 10a) or be oxidised further by O_3 or NO_3 to CH_3SO_3 (reaction 10b,c). CH_3SO_3 itself can react to form MSA (reaction 11a). CH_3SO_3 can also decompose to SO_3, similar to the decomposition reaction of CH_3SO_2, although it is assumed that this reaction is more endothermic (Barone et al., 1995). The rate constant cited by von Glasow and Crutzen (2004) that was previously implemented in CS2, could not be found in the cited primary literature (reaction 11b_old). Here, the rate constant of the decomposition reaction was updated to the rate constant used in the MCMv3.3.1, which is — as for the decomposition of CH_3SO_2 — based on Barone et al. (1995). We note that a more recent study, by Cao et al. (2013), calculates the rate constant for the thermal decomposition of CH_3SO_3 to be 12 s^{-1}; a factor of 80 larger than the value adopted here based on the MCMv3.3.1.

MSA is formed either through oxidation of MSIA (reaction 9b) or through the reaction of HO_2 with CH_3SO_3 (reaction 11a). The default configuration of UKCA (for example as run in UKESM1) does not include any sinks for MSA and it is not treated as a species, which prevents the comparison of MSA concentrations with observational results. Here, wet deposition of MSA is added with a Henry's law coefficient of 1×10^9 M atm^{-1} (Campolongo et al., 1999; Sander 2021). We note that Wollesen de Jonge et al. (2021) calculated the Henry's law coefficient to be approximately an order of magnitude lower and so this might be an overestimate. Dry deposition for MSA is added based on the implemented values for HCOOH in CRI. Additionally, the gas-phase oxidation of MSA by OH is added. Barnes et al. (2006) suggest this pathway is expected to play a minor role.

Wet deposition was added for MSIA with Henry's law constant of 1×10^8 M atm^{-1} (Barnes et al., 2006). Dry deposition is omitted for DMSO and MSIA since they are expected to be relatively short-lived.

S.1.2.1 The addition of the isomerization branch

Following the discovery of HPMTF (Veres et al., 2020) the pathway forming this molecule has now been well established (Wu et al., 2015; Veres et al., 2020; Berndt et al., 2019; Ye et al., 2021). The reactions of the isomerization branch that were added to CS2 (summarised in **Figure 1** and **Table 3**) were identified as those most important in determining SO_2 and HPMTF concentrations through sensitivity studies conducted using our box model setup. Details of these box model sensitivity studies

(and the discarded reaction pathways that were found to not be significant) are included in the supplement. In this sense, species like $HOOCH_2SCH_2OOH$, included in the studies by Khan et al. (2021) were neglected from our mechanism as this was found to have minor impact on the SO_2 and HPMTF simulated in the box model experiments. The reactions that were added include the autoxidation of MTMP to HPMTF in one step (reaction 2d) and the oxidation of HPMTF by OH, forming OCS (reaction 13b) and $HOOCH_2S$ (reaction 13a) with further oxidation to SO_2 (reactions 14-16). The equilibrium with the O_2-adduct, $HOOCH_2SOO$, and its subsequent decomposition (reaction 14c, 15a,b) was included with kinetics equivalent to CH_3SOO (reaction 5c, 6a,b). Photolysis was found to be a minor pathway of HPMTF loss in our marine boundary layer box model setup (< 10%) and was omitted from the final mechanism used here; contrary to the importance of photolysis of HPMTF found by Khan et al. (2021).

Dry deposition of HPMTF is set using the same parameters in UKCA as other soluble gas-phase compounds, such as CH_3OOH and H_2O_2, which yield an average deposition velocity similar to the observations of Vermeuel et al. (2020) of 0.75 cms^{-1}. For wet deposition of HPMTF, the Henry's law coefficient calculated by Wollesen de Jonge et al. (2021) was used.

For the sensitivity runs described in **Table 1**, some changes are made to the values in **Table 3**. In DMS-HPMTF-FP, the rate constant of reaction 2d is scaled by a factor of 5.0: Berndt et al. (2019) experimentally determined the rate constant at 295 K as 0.23 s^{-1}. Here the A-factor is scaled to match this value, while keeping the temperature dependence calculated by Veres et al. (2020) (following Wollesen de Jonge et al. (2021)). DMS-HPMTF-FL uses a rate constant 5.5 times faster for the total loss of HPMTF to OH (reaction 13a,b), which was recommended as an upper bound by Vermeuel et al. (2020) and following Khan et al. (2021). This range, between the base rate constant and the faster loss, puts us in the middle of the value experimentally determined by Ye et al. (2022). In the remaining sensitivity run CS2-HPMTF-CLD, heterogeneous uptake to both clouds and aerosols was added with reactive uptake coefficient (γ) of 0.01 (following Novak et al., 2021).

S1.3 Reduction of the HPMTF pathway

HPMTF can have more side reactions than are described in the main paper. Originally, a range of possible reactions were considered based on the literature and reactions that similar molecules undergo (Figure S1, Table S3). Reactions that were assessed include photolysis reactions and aqueous loss of HPMTF as well as reactions of the intermediate formed after the first isomerization step and the oxidation of this by HO_2 and NO, as described by Veres et al. (2020). In the SI, this scheme is referred to as CS2-HPMTF-compl.

To reduce computational time, as few reactions as possible should be included in a mechanism. At the same time, enough reactions need to be included so that the mechanism can faithfully reproduce the time evolution of the

species it models. The reactions which are removed from the mechanism should not play a significant role under the majority of atmospheric conditions. In this section, it is tested whether some of the reactions proposed can be removed without changing the concentration of key species. In this case the key species chosen were HPMTF and SO_2 (i.e. the mechanism was optimized to these species) because observational measurements exist for those species.

The BOXMOX runs were set up as described in Section 2.1.1 of the main paper. In the sensitivity runs, temperature, aerosol surface area, and O_3 and NO concentrations are varied to represent a diverse set of possible atmospheric conditions (Table S4). Figure S2 shows how the mean values of SO_2 and HPMTF concentration respond to the changing conditions in the CS2-HPMTF-compl scheme. Similar trends can be observed with minimum and maximum concentrations, although they are not explicitly shown here. When reactions are removed from the scheme, the response of SO_2 and HPMTF concentration to changing conditions should be maintained. The reduced CS2-HPMTF scheme will be referred to as CS2-HPMTF-red.

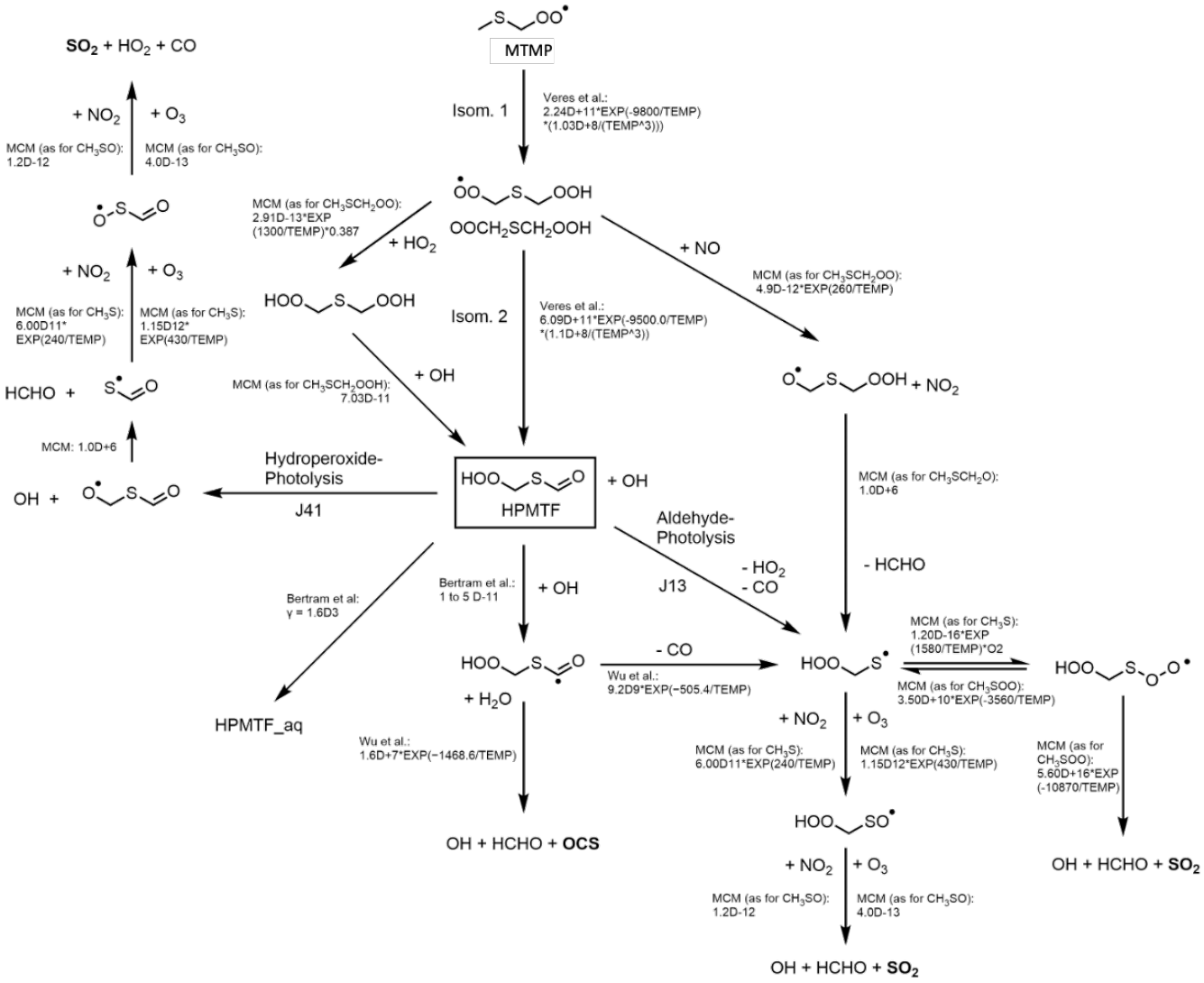

Figure S1: Complete isomerization pathway of HPMTF that was considered before reducing the mechanism.

Table S3: The complete isomerization pathway, referred to as CS2-HPMTF-compl.

No.	Reaction	Rate (cm^3 $molecule^{-1}$ s^{-1})	Reference
s1	$MTMP \rightarrow OOCH_2SCH_2OOH$	see note[a]	Veres et al. (2020)
s2a	$OOCH_2SCH_2OOH \rightarrow HPMTF + OH$	See note[b]	Veres et al. (2020)
s2b	$OOCH_2SCH_2OOH + HO2 \rightarrow HOOCH_2SCH_2OOH$	$1.13\times10^{-13}\ exp^{(1300/T)}$	Veres et al. (2020)
s3	$HOOCH_2SCH_2OOH + OH \rightarrow HPMTF$	7.03×10^{-11}	this work (like CH_2SCH_2OOH in MCMv3.3.1)

s2c	$OOCH_2SCH_2OOH + NO \rightarrow OCH2SCH2OOH + NO_2$	$4.90\times10^{-12}\,exp^{(260/T)}$	Veres et al. (2020)
s4	$OCH2SCH2OOH \rightarrow HOOCH2S + HCHO$	$1.0\times10^{+6}$	Veres et al. (2020)
s5a	$HPMTF + OH \rightarrow HOOCH_2S + H_2O + CO$	$1.0\times10^{-11} \times 0.9$	this work
s5b	$HPMTF + OH \rightarrow OCS + OH + HCHO + H_2O$	$1.0\times10^{-11} \times 0.1$	this work
s5c	$HPMTF \rightarrow HOOCH_2S + HO_2 + CO$	*J13*	this work
s5d	$HPMTF \rightarrow OCH_2SCHO + OH$	*J41*	this work
s5e	$HPMTF \rightarrow$ loss	gamma=0.1	this work
s6a	$HOOCH_2S + O_3 \rightarrow HOOCH_2SO$	$1.15\times10^{-12}\,exp^{(430/T)}$	Wu et al. (2015)
s6b	$HOOCH_2S + NO_2 \rightarrow HOOCH_2SO + NO$	$6.00\times10^{-11}\,exp^{(240/T)}$	Wu et al. (2015)
s6c	$HOOCH_2S + O_2 \rightarrow HOOCH_2SOO$	$1.20\times10^{-16}exp^{(1580/T)} \times [O_2]$	this work (like CH_3S)
s7a	$HOOCH_2SOO \rightarrow HOOCH_2S + O_2$	$3.50\times10^{+10}\,exp^{(-3560/T)}$	this work (like CH_3SOO)
s7b	$HOOCH_2SOO \rightarrow HCHO + OH + SO_2$	$5.60\times10^{+16}\,exp^{(-10870/T)}$	this work (like CH_3SOO)
s8a	$HOOCH_2SO + O_3 \rightarrow HCHO + OH + SO_2$	4×10^{-13}	Wu et al. (2015)
s8b	$HOOCH_2SO + NO_2 \rightarrow HCHO + OH + NO + SO_2$	1.2×10^{-11}	Wu et al. (2015)
s10	OCH2SCHO = HCHO + SCHO	$1.0\times10^{+6}$	this work (like s4)
s11a	$SCHO + O_3 = OSCHO$	$1.15\times10^{-12}\,exp^{(430/T)}$	this work (like s6a)
s11b	$SCHO + NO_2 = OSCHO + NO$	$6.00\times10^{-11}\,exp^{(240/T)}$	this work (like s6b)
s12a	$OSCHO + O_3 = SO_2 + HO_2 + CO$	4×10^{-13}	this work (like s8a)
s12b	$OSCHO + NO_2 = SO_2 + HO_2 + CO + NO$	1.2×10^{-11}	this work (like s8b)

[a] $2.24\times10^{+11}\,exp^{(-9800/T)}\,exp^{(1.03e8/(T\times T\times T))}$
[b] $6.09\times10^{+11}\,exp^{(-9500/T)}\,exp^{(1.1e8/(T\times T\times T))}$

Table S4: Conditions for sensitivity runs. For the NOx sensitivity run, NO, NO_2, and HNO_3 were varied to achieve NOx concentrations between 0.4 ppt and 4.4 ppb.

Sensitivity run	Temperature (K)	NO (ppt)	NO_2 (ppt)	HNO_3 (ppb)	O_3 (ppb)	Aerosol surface area ($\mu m^2\ cm^{-3}$)
Temp	260 - 310	1	10	0.5	30	15
NOx	290	0.1 - 1000	1 - 10,000	0.01 - 100	30	15
O_3	290	1	10	0.5	10 - 80	15
Aerosol	290	1	10	0.5	30	0 - 100

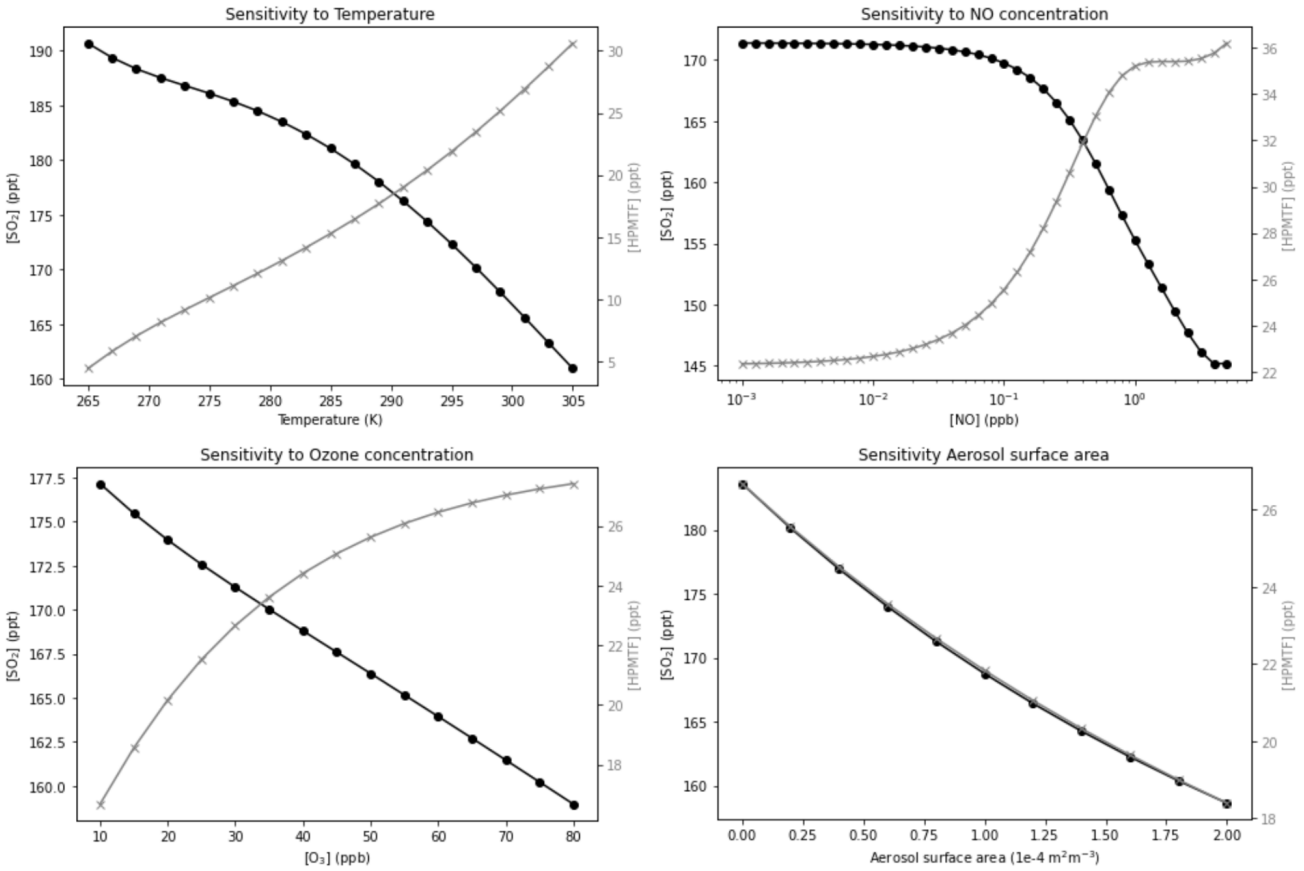

Figure S2: Sensitivity of mean SO_2 (black) and HPMTF (grey) concentration with the complete mechanism to the variation of temperature, NO and O_3 concentration, and aerosol surface area.

Removal of aldehyde and hydroperoxide photolysis of HPMTF (reactions s5c and s5d) has a negligible influence on HPMTF and SO_2 concentration (Figure S3) under the conditions simulated in the BOXMOX runs. This result is slightly at odds with the work of Khan et al. (2022), who found that photolysis was a dominant loss process. But in line with the work of Novak et al. (2022). The relative difference in HPMTF between CS2-HPMTF-compl and CS2-HPMTF-red is never higher than 6%. For SO_2 the maximum difference is 2% in total. In comparison: if OH-oxidation of HPMTF had been removed, mean SO_2 concentration at high temperatures would have dropped by more than 25% compared to CS2-HPMTF-red. Additionally, the large uncertainty regarding the rate of OH-oxidation is expected to have a much higher influence than the (non)inclusion of the photolysis reactions.

Therefore, reactions s5c and s5d and their plausible follow-up reactions are not included in the final CS2-HPMTF mechanism.

The effect of the removal of the two side reactions s2b and s3c after the first isomerization step of MSP, can be observed in Figure S4. At no point does SO_2 concentration change by more than 1% and HPMTF concentration does not vary by more than 5%. The minor role of both pathways was expected, since the second isomerization step s3 was calculated to be approximately a magnitude faster than the first isomerization step s2a (Wu et al., 2015, Veres et al., 2020). These side reactions have therefore also been excluded from the final mechanism.

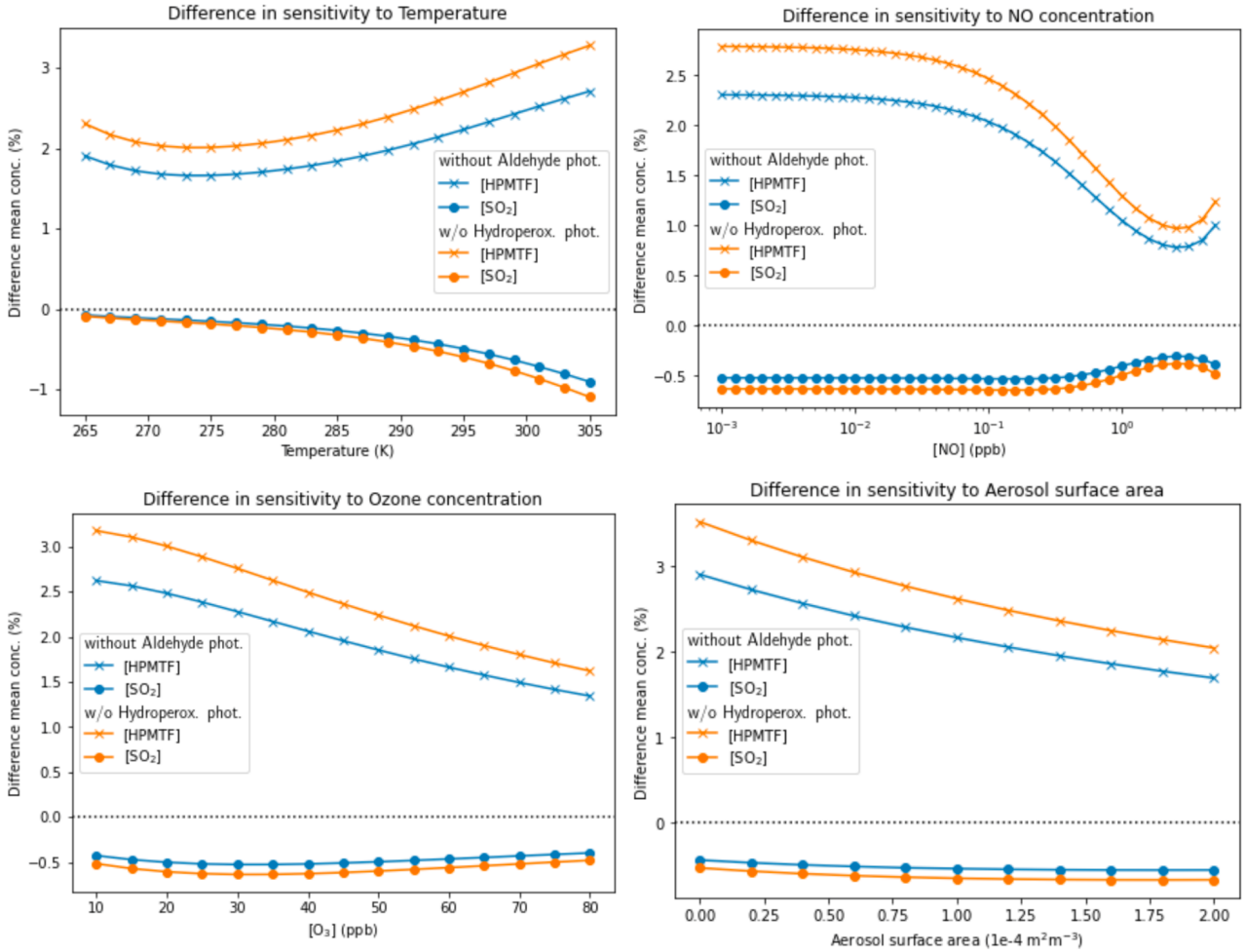

Figure S3: Difference in sensitivity of mean SO_2 and HPMTF concentration after the removal of the photooxidation reactions, compared to the complete mechanism.

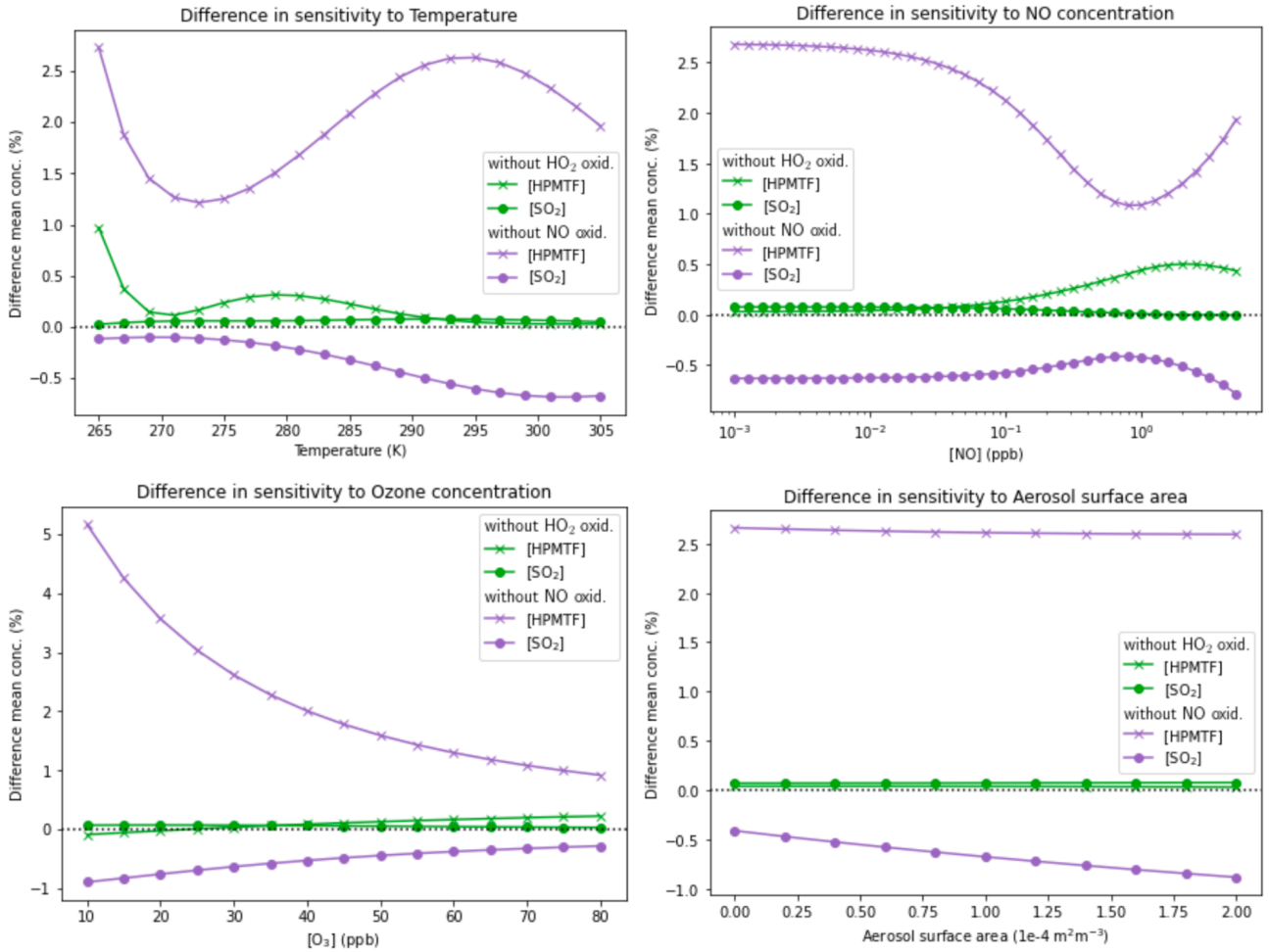

Figure S4: Difference in sensitivity of mean SO_2 and HPMTF concentration after the removal of the side reactions after the first isomerization step during HPMTF formation, compared to the complete mechanism

S1.3 Other BOXMOX plots

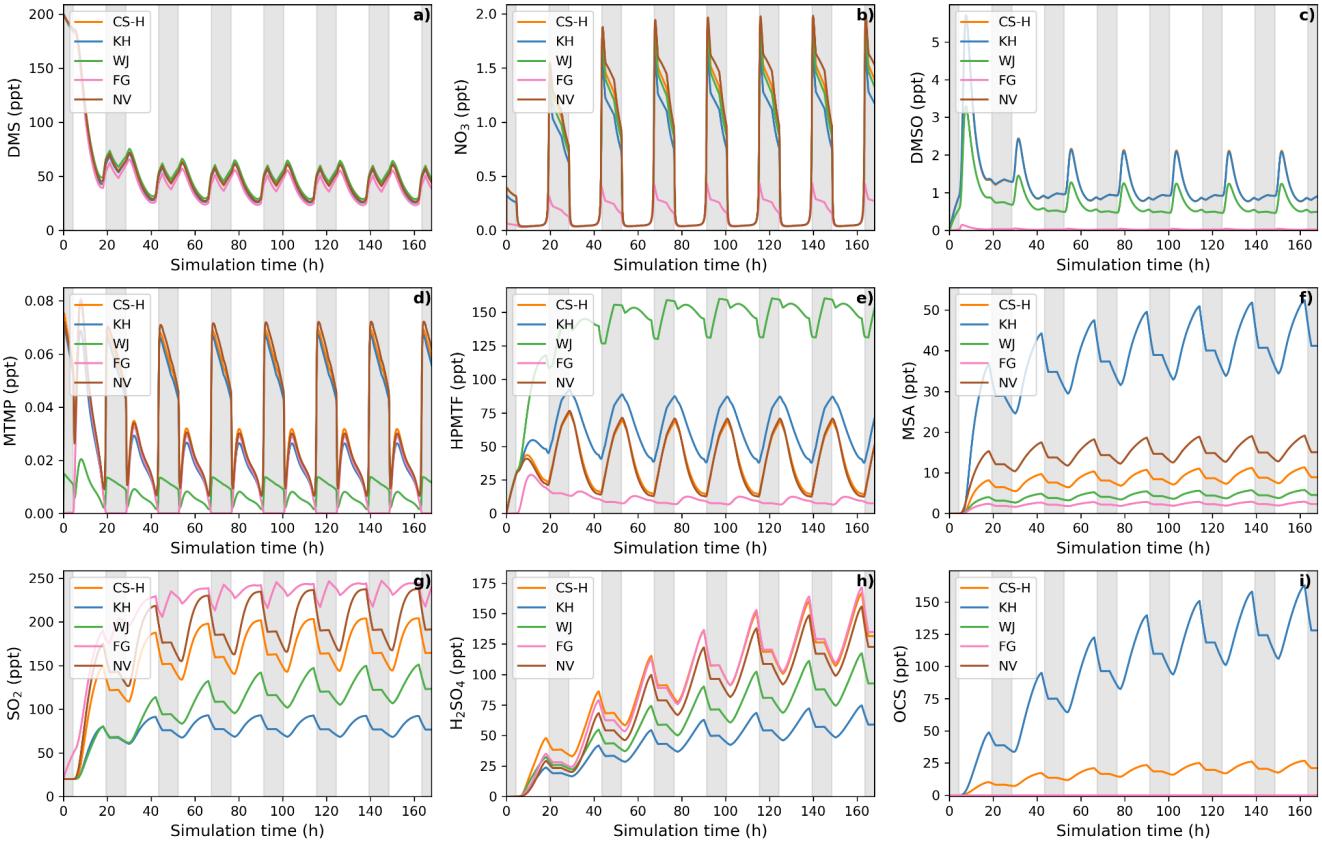

Figure S5: gas-phase concentrations as a function of time for different DMS gas-phase oxidation schemes used in UKCA configurations (oxidation by OH and NO_3). Grey areas denote nighttime, when no photolysis reactions are taking place. Average NOx concentration is approximately 100 ppt, with an average temperature of 293 K (range: 289 - 297 K).

S1.4 DMS schemes

S1.4.1 StratTrop (Archibald et al. 2020)

DMS + OH = SO2 : 1.20D-11*EXP(-260/TEMP) ;
DMS + OH = MSA + SO2 : 3.36224D-43*EXP(350/TEMP)*EXP(7460/TEMP)*M/(1+1.106D-31*EXP(7460/TEMP)*M) ;
DMS + NO3 = SO2 : 1.90D-13*EXP(500/TEMP) ;
DMS + O3P = SO2 : 1.30D-11*EXP(410/TEMP) ;

S1.4.2 Wollesen de Jonge et al. (2021)

DMS + NO3 = CH3SCH2O2 + HNO3 : 1.9D-13*exp(520/TEMP) ;
DMS + OH = CH3SCH2O2 : 1.12D-11*exp(-250/TEMP) ;
DMS + OH = CH3SOHCH3 : 9.5D-39*O2*EXP(5270/TEMP)/(1+7.5D-29*O2*EXP(5610/TEMP)) ;
CH3SOHCH3 = HODMSO2 : 8.5D-13*O2 ;
CH3SOHCH3 = CH3SOH + CH3O2 : 5D+5 ;
CH3SOHCH3 = DMS + OH : (2.048D-14*O2*exp(2674/TEMP)/(1+5.5D-31*O2*exp(7640/TEMP)))/(TEMP) ;
CH3SOH + OH = CH3SO : 5D-11 ;
CH3SCH2O2 + HO2 = CH3SCH2OOH : KRO2HO2*0.387 ;
CH3SCH2O2 + NO = CH3SCH2O + NO2 : 4.9D-12*exp(260/TEMP) ;
CH3SCH2O2 + NO3 = CH3SCH2O + NO2 : KRO2NO3 ;
CH3SCH2O2 = CH3SCH2O : 2*(K298CH3O2*1.0D-11)**0.5*RO2*0.8 ;
CH3SCH2O2 = CH3SCH2OH : 2*(K298CH3O2*1.0D-11)**0.5*RO2*0.1 ;
CH3SCH2O2 = CH3SCHO : 2*(K298CH3O2*1.0D-11)**0.5*RO2*0.1 ;
CH3SCH2OOH + OH = CH3SCHO + OH : 7.03D-11 ;
CH3SCH2OOH = CH3SCH2O + OH : (5.786D-6)*SUN ;
CH3SCH2O = CH3S + HCHO : KDEC ;
CH3SCH2OH + OH = CH3SCHO + HO2 : 2.78D-11 ;
CH3SCHO + OH = CH3S + CO : 1.11D-11 ;
CH3SCHO = CH3S + CO + HO2 : (1.99D-5)*SUN ;
CH3SCH2O2 = OOCH2SCH2OOH : 2.2433D11*exp(-9.8016D3/TEMP)*exp(1.0348D8/(TEMP*TEMP*TEMP))*5 ;
OOCH2SCH2OOH = HPMTF + OH : 6.097D11*exp(-9.4892D3/TEMP)*exp(1.102D8/(TEMP*TEMP*TEMP)) ;
OOCH2SCH2OOH + NO = HOOCH2S + NO2 + HCHO : 4.9D-12*exp(260/TEMP) ;
OOCH2SCH2OOH + HO2 = HOOCH2SCH2OOH : 1.13D-13*exp(1300/TEMP) ;
HPMTF + OH = HOOCH2SCO : 1.4D-12 ;
HOOCH2SCO = HOOCH2S + CO : 9.2D9*exp(-505.4/TEMP) ;
HOOCH2SCO = HCHO + OH + OCS : 1.6D7*exp(-1468.6/TEMP) ;
HOOCH2S + O3 = HOOCH2SO : 1.15D-12*exp(430/TEMP) ;

HOOCH2S + NO2 = HOOCH2SO + NO : 6.00D-11*exp(240/TEMP) ;
HOOCH2SO + O3 = SO2 + HCHO + OH : 4.00D-13 ;
HOOCH2SO + NO2 = SO2 + HCHO + OH + NO : 1.20D-11 ;
CH3S + NO2 = CH3SO + NO : 6.00D-11*exp(240/TEMP) ;
CH3S + O3 = CH3SO : 1.15D-12*exp(430/TEMP) ;
CH3S = CH3SOO : 1.20D-16*exp(1580/TEMP)*O2 ;
CH3SO + NO2 = CH3O2 + SO2 + NO : 1.20D-11*0.25 ;
CH3SO + NO2 = CH3SO2 + NO : 1.20D-11*0.75 ;
CH3SO + O3 = CH3O2 + SO2 : 4.00D-13 ;
CH3SO = CH3SOO2 : 3.12D-16*exp(1580/TEMP)*O2 ;
CH3SOO + NO = CH3SO + NO2 : 1.1D-11 ;
CH3SOO + NO2 = CH3SO + NO3 : 2.2D-11 ;
CH3SOO = CH3O2 + SO2 : 5.60D+16*exp(-10870/TEMP) ;
CH3SOO = CH3S : 3.50D+10*exp(-3560/TEMP) ;
CH3SOO + HO2 = CH3SOOH : 4D-12 ;
CH3SOO = CH3SO2 : 1.0 ;
CH3SOO2 + HO2 = CH3SO2 + OH : KAPHO2*0.44 ;
CH3SOO2 + HO2 = CH3SOOOH :KAPHO2*0.41 ;
CH3SOO2 + HO2 = MSIA + O3 : KAPHO2*0.15 ;
CH3SOO2 + NO = CH3SO2 + NO2 : 1.00D-11 ;
CH3SOO2 + NO2 = CH3SOO2NO2 : 1.20D-12*(TEMP/300)**(-0.9) ;
CH3SOO2 + NO3 = CH3SO2 + NO2 : KRO2NO3*1.74 ;
CH3SOO2 = CH3SO : 9.10E+10*exp(-3560/TEMP) ;
CH3SOO2 = CH3SO2 : 1.00D-11*RO2*0.7 ;
CH3SOO2 = MSIA : 1.00D-11*RO2*0.3 ;
CH3SOOOH + OH = CH3SOO2 : 9.00D-11 ;
CH3SOOOH = CH3SO2 + OH : (5.786D-6)*SUN ;
CH3SOO2NO2 + OH = MSIA + NO2 : 1.00D-11 ;
CH3SOO2NO2 = CH3SOO2 + NO2 : 5.40D+16*exp(-13112/TEMP) ;
CH3SO2 + O3 = CH3SO3 : 3.00D-13 ;
CH3SO2 = CH3O2 + SO2 : 5.00D+13*exp(-9673/TEMP) ;
CH3SO2 = CH3SO2O2 : 1.03D-16*exp(1580/TEMP)*O2 ;
CH3SO2 + OH = MSA : 5D-11 ;
CH3SO2 + NO2 = CH3SO3 + NO : 2.2D-11 ;
CH3SO2O2 + HO2 = CH3SO2OOH : KAPHO2*0.41 ;
CH3SO2O2 + HO2 = CH3SO3 + OH : KAPHO2*0.44 ;
CH3SO2O2 + HO2 = MSA + O3 : KAPHO2*0.15 ;
CH3SO2O2 + NO = CH3SO3 + NO2 : 1.00D-11 ;
CH3SO2O2 + NO2 = CH3SO4NO2 : 1.20D-12*(TEMP/300)**(-0.9) ;

CH3SO2O2 + NO3 = CH3SO3 + NO2 : KRO2NO3*1.74 ;
CH3SO2O2 = CH3SO2 : 3.01D+10*exp(-3560/TEMP) ;
CH3SO2O2 = CH3SO3 : 1.00D-11*RO2*0.7 ;
CH3SO2O2 = MSA : 1.00D-11*RO2*0.3 ;
CH3SO3 + HO2 = MSA : 5.00D-11 ;
CH3SO3 = CH3O2 + SO3 : 5.00D+13*exp(-9946/TEMP) ;
CH3SO2OOH + OH = CH3SO2O2 : 3.60D-12 ;
CH3SO2OOH = CH3SO3 + OH : (5.786D-6)*SUN ;
CH3SO4NO2 + OH = CH3SO2O2 + HNO3 : 3.60D-13 ;
CH3SO4NO2 = CH3SO2O2 + NO2 : 5.40D+16*exp(-13112/TEMP) ;
HODMSO2 + NO = DMSO2 + HO2 + NO2 : KRO2NO ;
HODMSO2 = DMSO + HO2 : 8.90E+10*exp(-6040/TEMP) ;
DMSO + OH = MSIA + CH3O2 : 6.10D-12*exp(800/TEMP) ;
DMSO + NO3 = DMSO2 + NO2 : 2.9D-13 ;
DMSO2 + OH = DMSO2O2 : 4.40D-14 ;
DMSO2O2 + HO2 = DMSO2OOH : KRO2HO2*0.387 ;
DMSO2O2 + NO = DMSO2O + NO2 : KRO2NO ;
DMSO2O2 + NO3 = DMSO2O + NO2 : KRO2NO3 ;
DMSO2O2 = CH3SO2CHO : 2.00D-12*RO2*0.2 ;
DMSO2O2 = DMSO2O : 2.00D-12*RO2*0.6 ;
DMSO2O2 = DMSO2OH : 2.00D-12*RO2*0.2 ;
DMSO2OOH + OH = CH3SO2CHO + OH : 1.26D-12 ;
DMSO2OOH + OH = DMSO2O2 : 3.60D-12 ;
DMSO2OOH = DMSO2O + OH : (5.786D-6)*SUN ;
DMSO2O = CH3SO2 + HCHO : KDEC ;
DMSO2OH + OH = CH3SO2CHO + HO2 : 5.23D-13 ;
DMSO2OH + OH = DMSO2O : 1.40D-13 ;
CH3SO2CHO + OH = CH3SO2 + CO : 1.78D-12 ;
CH3SO2CHO = CH3SO2 + CO + HO2 : (1.99D-5)*SUN ;
MSIA + OH = CH3SO2 : 1D-10 ;
MSIA + NO3 =CH3SO2 + HNO3 : 1D-13 ;
MSA + OH = CH3SO3 : 2.24D-14 ;

S1.4.3 Fung et al. (2021)

DMS + OH = MTMP: 1.12D-11*EXP(-250/TEMP) ;
MTMP + NO = CH3SCH2O + NO2 : 4.90D-12*EXP(260/TEMP) ;
MTMP = CH3SCH2O + O2 : 3.74D-12*RO2 ;
CH3SCH2O = CH3S +HCHO : 1.00D+6 ;
CH3S + O3 = CH3SO + O2 : 1.15D-12*EXP(430/TEMP) ;

CH3S + O2 = CH3SOO : 1.20D-16*EXP(1580/TEMP)*O2 ;
CH3SO + O3 = CH3O2 + SO2 : 4.0D-13 ;
CH3SOO = CH3O2 + SO2 : 5.60D+16*EXP(-10870/TEMP) ;
CH3SOO = CH3SO2 : 1.00 ;
CH3SO2 + O3 = CH3SO3 + O2 : 3.0d-13 ;
CH3SO2 = CH3O2 + SO2 : 5.00D13*EXP(-9673/TEMP) ;
CH3SO3 + HO2 = MSA + O2 : 5.0d-11 ;
CH3SO3 = CH3O2 + H2SO4 : 5.00D+13*EXP(-9946/TEMP) ;
MTMP= OOCH2SCH2OOH : 2.24D+11*EXP(-9800/TEMP)*EXP(1.03D+8/(TEMP*TEMP*TEMP)) ;
OOCH2SCH2OOH = HPMTF + OH : 6.09D+11*EXP(-9500.0/TEMP)*EXP(1.1D+8/(TEMP*TEMP*TEMP)) ;
OOCH2SCH2OOH + NO = OCH2SCH2OOH + NO2 : 4.9D-12*EXP(260/TEMP) ;
OCH2SCH2OOH = HOOCH2S + HCHO : 1.00D+6 ;
OOCH2SCH2OOH + HO2 = HOOCH2SCH2OOH + O2 : 1.13D-13*EXP(1300/TEMP) ;
HPMTF + OH = HOOCH2SCO + H2O : 1.11D-11 ;
HOOCH2SCO = HOOCH2S + CO : 9.20D+9*EXP(-505.4/TEMP) ;
HOOCH2SCO = OH + HCHO + OCS : 1.60D+7*EXP(-1468.6/TEMP) ;
HOOCH2S + O3 = HOOCH2SO : 1.15D-12*EXP(430/TEMP) ;
HOOCH2S + NO2 = HOOCH2SO + NO : 6.00D-11*EXP(240/TEMP) ;
HOOCH2SO + O3 = HCHO + OH + SO2 : 4.0D-13 ;
HOOCH2SO + NO2 = SO2 + HCHO + OH + NO : 1.2d-11;
DMS + OH = SO2 + CH3O2 : 8.2D-39*O2*EXP(5376/TEMP)/(1+7.5D-5*(O2/M)*EXP(3644/TEMP))*0.6 ;
DMS + OH = DMSO + CH3O2 : 8.2D-39*O2*EXP(5376/TEMP)/(1+7.5D-5*(O2/M)*EXP(3644/TEMP))*0.4 ;
DMS + NO3 = SO2 + HNO3 + CH3O2 + HCHO : 1.13D-12*EXP(530/TEMP) ;
DMSO + OH = MSIA : 8.94D-11*EXP(800/TEMP)*0.95 ;
DMSO + OH = SO2 : 8.94D-11*EXP(800/TEMP)*0.05 ;
MSIA + OH = SO2 : 9.00D-11*0.9 ;
MSIA + OH = MSA : 9.00D-11*0.1 ;
MSIA + O3 = MSA : 2.00D-18 ;
MSIA + O3 = MSA : 2.00D–18 ;

S1.4.4 Khan et al. (2021)

DMS + OH = MTMP+ H2O : 1.2D-11*EXP(-280/TEMP) ;
DMS + OH = DMSO + HO2 : 9.5D-39*O2*EXP(5270/TEMP)/(1+7.5D-29*O2*EXP(5610/TEMP)) ;
DMS + NO3 = MTMP + HNO3 : 1.90D-13*EXP(580/TEMP) ;
MTMP + NO = HCHO + CH3S + NO2 : 4.90D-12*EXP(260/TEMP) ;
MTMP + MTMP = HCHO + HCHO + CH3S + CH3S : 1.0d-11 ;
MTMP + HO2 = CH3SCH2OOH: 2.9D-13*EXP(1300/TEMP) ;
CH3SCH2OOH = CH3S + HCHO + OH: (5.78677D-6)*SUN ; {J41}
CH3SCH2OOH + OH = CH3SCHO + OH: 7.0D-11 ;

CH3SCHO + OH = CH3S + CO : 1.1D-11 ;
CH3SCHO = CH3S + CO + HO2 : (1.99124D-5)*SUN ;
CH3S + O3 = CH3SO : 1.15D-12*EXP(430/TEMP) ;
CH3S + NO2 = CH3SO + NO : 3.00D-12*EXP(210/TEMP) ;
CH3SO + NO2 = CH3SO2 + NO : 1.2d-11*0.82 ;
CH3SO + NO2 = SO2 + CH3O2 + NO : 1.2d-11*0.18 ;
CH3SO + O3 = CH3SO2 : 6.0d-13 ;
CH3SO2 = SO2 + CH3O2 : 5.00D13*EXP(-9673/TEMP) ;
CH3SO2 + NO2 = CH3SO3 + NO : 2.2d-12 ;
CH3SO2 + O3 = CH3SO3 : 3.0d-13 ;
CH3SO3 + HO2 = MSA : 5.0d-11 ;
CH3SO3 = CH3O2 + H2SO4 : 1.36D14*EXP(-11071/TEMP) ;
DMSO + OH = MSIA + CH3O2 : 8.7d-11*0.95 ;
MSIA + OH = CH3SO2 + H2O : 9.d-11*0.95 ;
MSIA + OH = MSA + HO2 + H2O : 9.d-11*0.05 ;
MSIA + NO3 = CH3SO2 + HNO3 : 1.0d-13 ;
MTMP = OOCH2SCH2OOH + O2: 2.74D+7*EXP(-5950/TEMP) ;
OOCH2SCH2OOH = HPMTF + OH: 4.2D+7*EXP(-5390/TEMP) ;
OOCH2SCH2OOH + NO = HOOCH2S + NO2 + HCHO : 4.9D-12*exp(260/TEMP) ;
OOCH2SCH2OOH + HO2 = HOOCH2SCH2OOH : 1.13D-13*exp(1300/TEMP) ;
HOOCH2SCH2OOH = HOOCH2S + HCHO + OH : (5.78677D-6)*SUN ; {J41}
HOOCH2SCH2OOH + OH = OOCH2SCH2OOH : 1.36D-11 ;
HPMTF + OH = HOOCH2S + CO : 1.4D-12*(5.6D-3*TEMP - 1.24) ;
HPMTF + OH = OH + HCHO + OCS : 1.4D-12*(1-(5.6D-3*TEMP - 1.24)) ;
HPMTF = HOOCH2S + CO + HO2: (5.78677D-6)*SUN ; {J41}
HPMTF = OCS + HCHO + OH: (2.0126D-5)*SUN; {J14}
HOOCH2S + O3 = HOOCH2SO : 1.15D-12*exp(430/TEMP) ;
HOOCH2S + NO2 = HOOCH2SO + NO : 6.00D-11*exp(240/TEMP) ;
HOOCH2SO + O3 = SO2 + HCHO + OH : 4.00D-13 ;
HOOCH2SO + NO2 = SO2 + HCHO + OH + NO : 1.20D-11 ;

S1.4.5 Novak et al. (2021)
DMS + OH = MTMP + H2O : 1.12D-11*EXP(-250/TEMP) ;
DMS + OH = SO2 : (8.2D-39*O2*EXP(5376/TEMP) / (1+ 1.05D5*EXP(3644/TEMP)*0.2095))*0.75 ;
DMS + OH = MSA : (8.2D-39*O2*EXP(5376/TEMP) / (1+ 1.05D-5*EXP(3644/TEMP)*0.2095))*0.25 ;
DMS + NO3 = MTMP + HNO3 : 1.90D-13*EXP(520/TEMP) ;
MTMP + HO2 = SO2 : 1.13D-13*EXP(1300/TEMP) ;
MTMP + RO2 = SO2 : 1.0D-11 ;
MTMP + NO = SO2 + NO2 : 4.9D-12*EXP(260/TEMP) ;

MTMP + NO3 = SO2 + NO2 : 2D-12 ;
MTMP = HPMTF : 2.24D+11*EXP(-9800/TEMP)*EXP(1.03D+8/(TEMP*TEMP*TEMP)) ;
HPMTF + OH = SO2 : 1.11D-11 ;

S1.4.6 CRIStrat2 (Weber et al. 2021; Archer-Nicholls et al. 2021)
DMS + OH = MTMP + H2O : 1.12D-11*EXP(-250/TEMP) ;
DMS + NO3 = MTMP + HNO3 : 1.90D-13*EXP(520/TEMP) ;
MTMP + NO = HCHO + MeS + NO2 : 4.9D-12*EXP(263/TEMP) ;
MTMP + MTMP = HCHO + HCHO + MeS + MeS : 1.10D-11 ;
MeS + O3 = MeSO : 1.15D-12*EXP(432/TEMP) ;
MeS + NO2 = MeSO + NO: 3.0D-12*EXP (210/TEMP) ;
MeSO + NO2 = 0.82*MeSO2 + NO + 0.18*SO2 + 0.18*CH3O2: 1.2D-11 ;
MeSO + O3 = MeSO2 : 6.0D-13 ;
MeSO2 = SO2 + CH3O2: 5.0D+13*EXP(-9763/TEMP) ;
MeSO2 + NO2 = MeSO3 + NO2 : 2.2D-12 ;
MeSO2 + O3 = MeSO3 : 3.0D-13 ;
MeSO3 + HO2 = MSA : 5.0D-11 ;
MeSO3 = CH3O2 + H2SO4 : 1.36D+14*EXP(-11071/TEMP) ;
DMSO + OH = 0.95*MSIA + 0.95*CH3O2 : 8.7D-11 ;
MSIA + OH = 0.95*MeSO2 + 0.925*MSA + 0.05*HO2 : 9.0D-11 ;
MSIA + NO3 = MeSO2 + HNO3 : 1.0D-13 ;
DMS + OH = DMSO + HO2 : KDMSO ;
Where KDMSO is equal to (6.5E−39 [O2] exp(5270/T))/(1 + 7.5E−29 [O2] exp(5610/T); where [O2] is the concentration of molecular oxygen in molecule cm^{-3}

S2 Global modelling with UKCA

S2.1 Additional information on the emissions and set up used in the UKCA modelling.

Anthropogenic and biomass burning emissions data (including DMS) for CMIP6 are from the Community Emissions Data System (CEDS), as described by Hoesly et al. (2018). All runs used time slice 2014 emissions for anthropogenic and biomass burning emissions. Oceanic emissions of CO, C_2H_4. C_2H_6, C_3H_6 and C_3H_8 were from the POET 1990 data set (Olivier et al., 2003), and all terrestrial biogenic emissions except isoprene and monoterpenes were based on 2001–2010 climatologies from Model of Emissions of Gases and Aerosols from Nature under the Monitoring Atmospheric Composition and Climate project (MEGAN-MACC) (MEGAN) version 2.1 (Guenther et al., 2012). Emissions of isoprene and monoterpenes were simulated by the interactive biogenic volatile organic compound (iBVOC) emissions system (Pacifico et al.. 2011), the standard approach for UKESM1's contributions to CMIP6 (Sellar et al., 2019). Emissions of isoprene and monoterpenes are calculated interactively based on temperature, CO_2, photosynthetic activity and plant functional types for each grid cell.

While the StratTrop mechanism and the variants of the CS2 mechanism all use the same raw emissions data, the additional emitted species required by CS2 means the total mass of emitted organic compounds is greater in CS2, and the lumping of species for emissions is also different. The approach and consequences are discussed in Archer-Nicholls et al (2021).

Nudging is used in the 3D model as this constrains the different simulations to consistent meteorology, thus preventing differences in meteorology complicating the attribution of differences resulting from the chemical mechanism changes, and replicating the atmospheric conditions experienced when the observations were recorded as closely as possible. Nudging only occurred above ~1200 m in altitude, and thus the majority of the planetary boundary layer was not nudged. The model runs were atmosphere-only runs with prescribed sea surface temperatures (SSTs). CO_2 is not emitted but set to a constant field, while methane, CFCs, and N_2O are prescribed with constant lower boundary conditions, all at 2014 levels (Archibald et al., 2020).

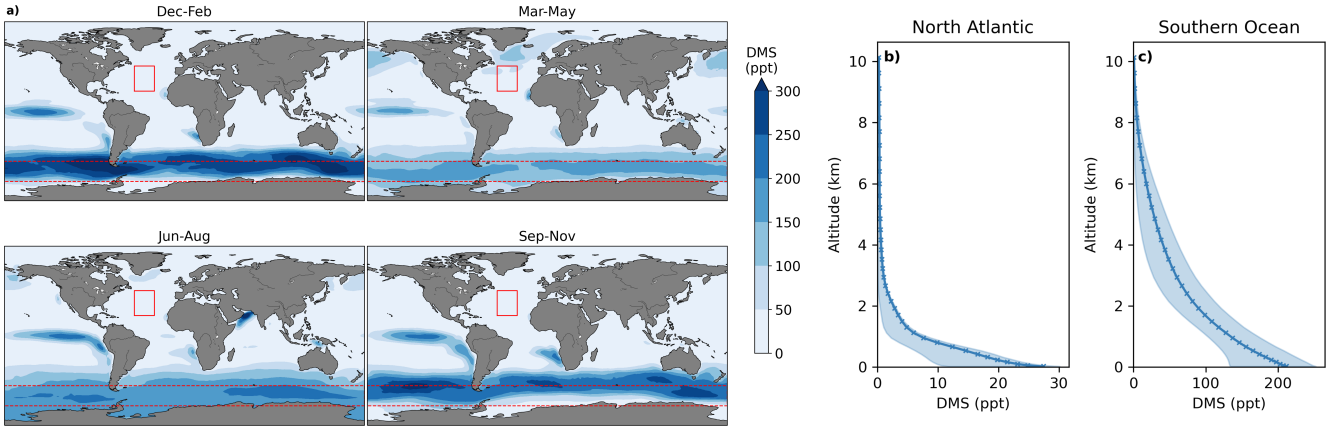

Figure S6: **a)** Global distribution of DMS mixing ratios in the lower troposphere (< 2 km) over the oceans in CS2. Annual mean vertical distribution of DMS in **b)** the Central North Atlantic (30-50°E, 20-45°N, denoted with the red rectangle in panel **a**) and in **c)** the Southern Ocean (50-70°S, denoted with the red dashed rectangle in panel **a**). The envelopes represent the interquartile range of the model simulation results. Note the order of magnitude difference in the DMS concentrations between the North Atlantic and Southern Ocean.

S2.1.1 Comparison of DMS with observations

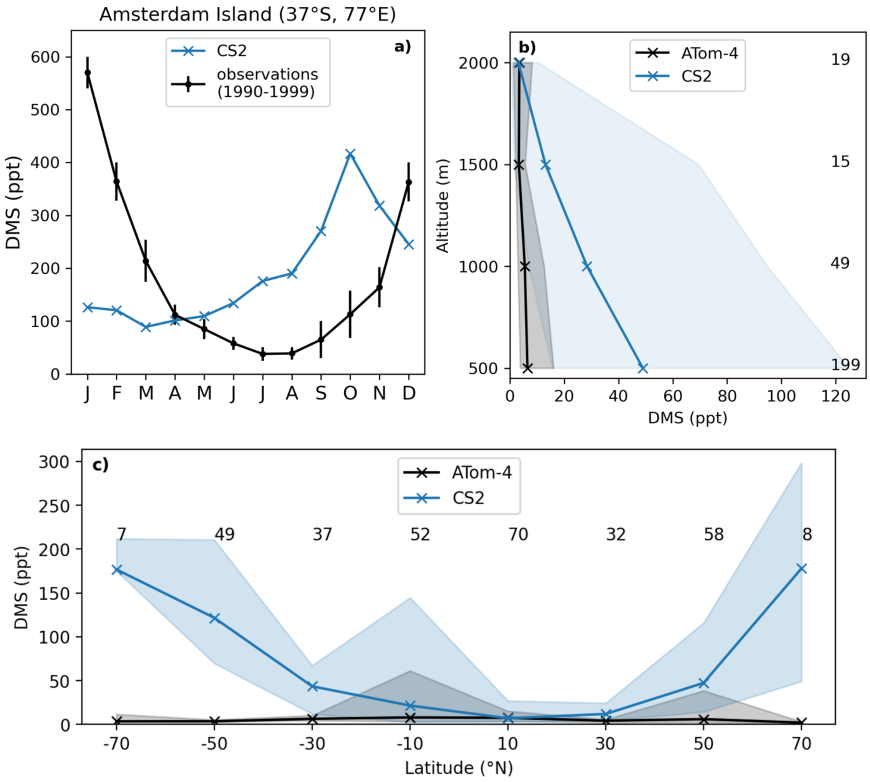

Figure S7: (a) Comparison of DMS surface concentration on Amsterdam Island (37°S, 77°E) in the southern Indian Ocean. The observational data (Sciare et al., 2000) represents the monthly mean concentrations and their standard deviations for the years 1990-1999. **(b)** Vertically binned (500 m) and **(c)** latitudinally binned (20°) median DMS mixing ratio along the Atom-4 flight path. The envelopes represent the interquartile range of the measurements and the respective model results while the numbers on the side/on top give the number of measurements in the respective bin. In b) and c) the model data are sampled along the Atom flight track using hourly mean model data.

DMS was not significantly affected by the different DMS mechanisms in the simulations with UKCA and so we focus on the results from the CS2 simulation. **Figure S7** compares observed DMS from ground based measurements on the Amsterdam Island and *in situ* measurements from the Atom-4 flights with the simulated DMS in CS2. On Amsterdam Island, a clear seasonality was observed for the monthly mean DMS concentration, with a peak during the austral summer (570 ppt) and a

minimum during the austral winter (38 ppt). The simulated DMS (89 – 416 ppt) falls within that range but fails to capture the observed seasonal trends (**Figure S7a**). We suggest that the disagreement between the observed and modelled atmospheric DMS mixing ratios is driven by the DMS emissions dataset we have applied in this study (similar to other recent DMS chemistry studies e.g., Fung et al. (2022)). Bock et al. (2021) reviewed CMIP6 DMS emissions and found that the emissions used in our study (from the UKESM-1 model) tend to result in less spatial heterogeneity than observational based climatologies (e.g., Lana et al. (2011)). During the tuning of the UEKSM-1 model (Sellar et al., 2019) the DMS emission scheme was modified to have a minimum DMS ocean concentration of 1nM imposed, the effect of which seems to be to generally overestimate the DMS emissions over the low productivity regions. Overall, we found the atmospheric DMS concentration in the model (which hitherto has not been evaluated before) to be significantly higher compared with the airborne observations from Atom-4 (**Figure S7b** and **S7c**). At the altitudes shown, the model predicts DMS approximately 5 times higher than the measurements. A comparison along the latitudinal axis (**Figure S7c**) reveals that DMS is significantly overestimated at high latitudes (however, it should be taken into account that only few measurements exist for latitudes above 60° from Atom4).

It is difficult to evaluate atmospheric DMS globally as there are limited observations that can be used for evaluating global models. For instance, Amsterdam Island being one of only a handful of long-term observational sites, no remote sensing-based data and with most atmospheric observations made on ships that are focusing on plumes of DMS. None the less, our CS2 base run (and all subsequent UKCA runs) suffer from a high bias in simulated atmospheric DMS, driven by the use of the emissions dataset we used. We opted to use the default UKESM DMS emissions as our focus in this study is the oxidation mechanism. However, we suggest that future work assess the impacts of both DMS emissions and chemistry using some of the more recent DMS emissions datasets (Gali et al., 2018; Hulswar et al., 2022).

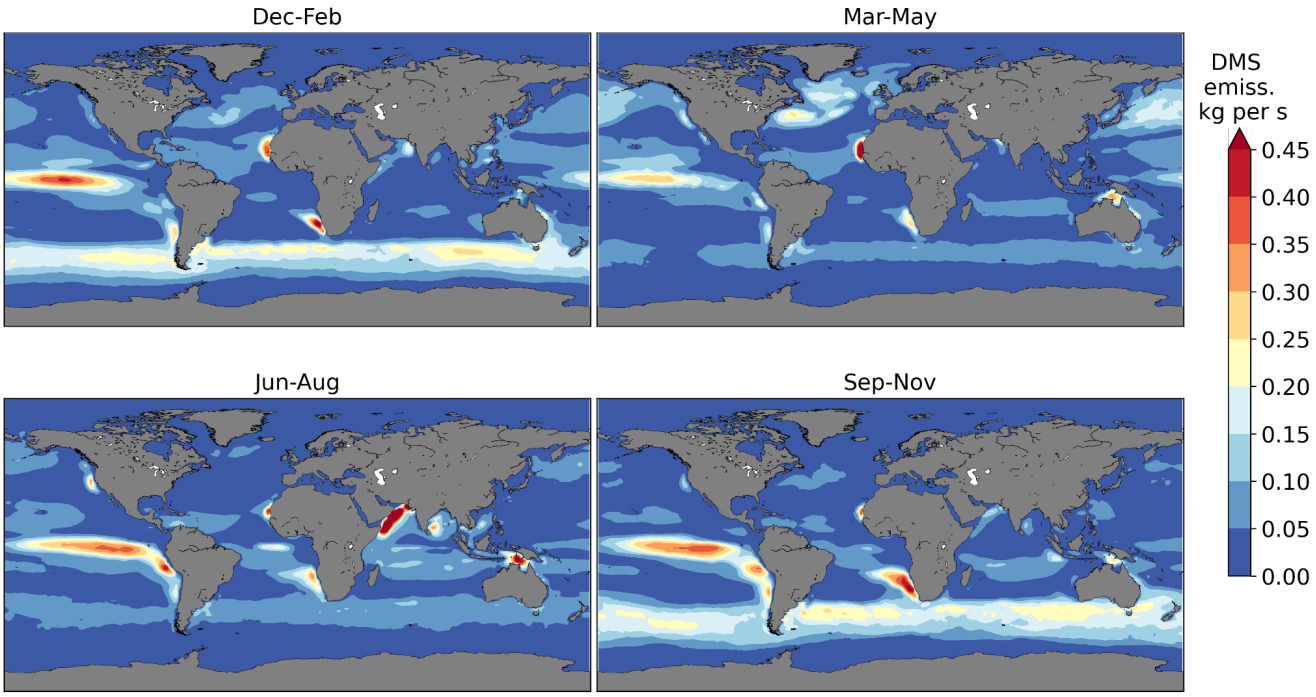

Figure S8: DMS emissions in CS2 and all simulations with UKCA.

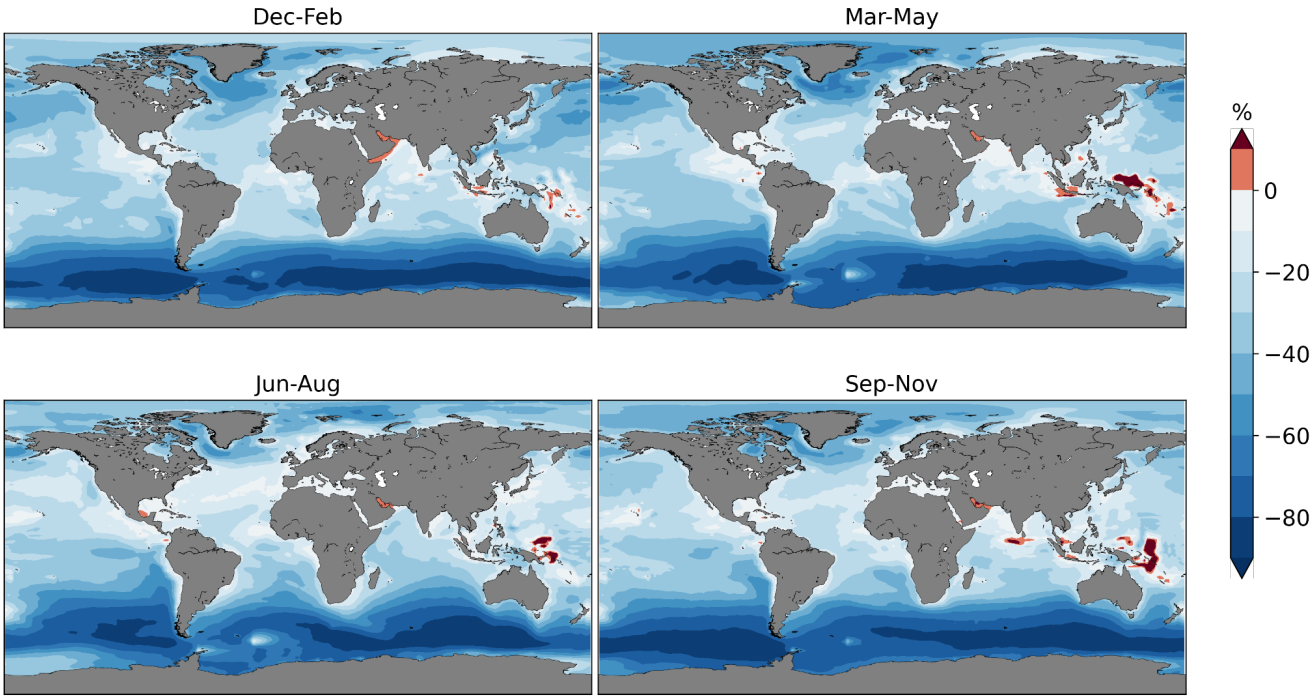

Figure S9: Relative difference in SO_2 mixing ratios in the lower troposphere (< 2 km) between CS2-HPMTF and the StratTrop run ST (CS2-HPMTF – ST). Only values above the ocean are shown.

S2.1.2 Modelled MSA

MSA is an important intermediate of the OH-addition channel. It contributes to aerosol growth and might play a role in new particle formation (Chen et al., 2015; Chen and Finlayson-Pitts, 2017). MSA production is reduced from 7.9 Tg S yr^{-1} in CS2 by 70% to 2.4 Tg S yr^{-1} in CS2-HPMTF. In the CS2-HPMTF simulation, wet and dry deposition and gas-phase oxidation by OH to CH_3SO_3 have been included as loss processes for MSA, which account for 89%, 10%, and 1% of the loss of MSA; respectively. The tropospheric MSA burden is 40 Gg S in CS2-HPMTF with a lifetime of 6 days.

In CS2-HPMTF, MSA is greatest in the Southern Ocean (**Figure S10**), where it shows a strong seasonal pattern, similar to DMS. Mixing ratios up to 80 ppt are reached in January (Austral summer), while in July they are below 10 ppt. This is reflected in the big interquartile range of MSA in the Southern Ocean (**Figure S10c**). Since the OH addition pathway is negatively temperature dependent, MSA is primarily produced at high latitudes, inversely to HPMTF. MSA shows the greatest asymmetry in concentration between the North Atlantic and Southern Ocean out of the different species discussed here. As well as significant differences between the magnitude of MSA simulated in the North Atlantic and Southern Ocean, the vertical profiles of MSA are shown to be very different. MSA reaches a peak in concentration at around 2 km altitude in the Southern Ocean (consistent with a longer DMS lifetime and therefore greater vertical transport), whereas it peaks near the surface in the North Atlantic.

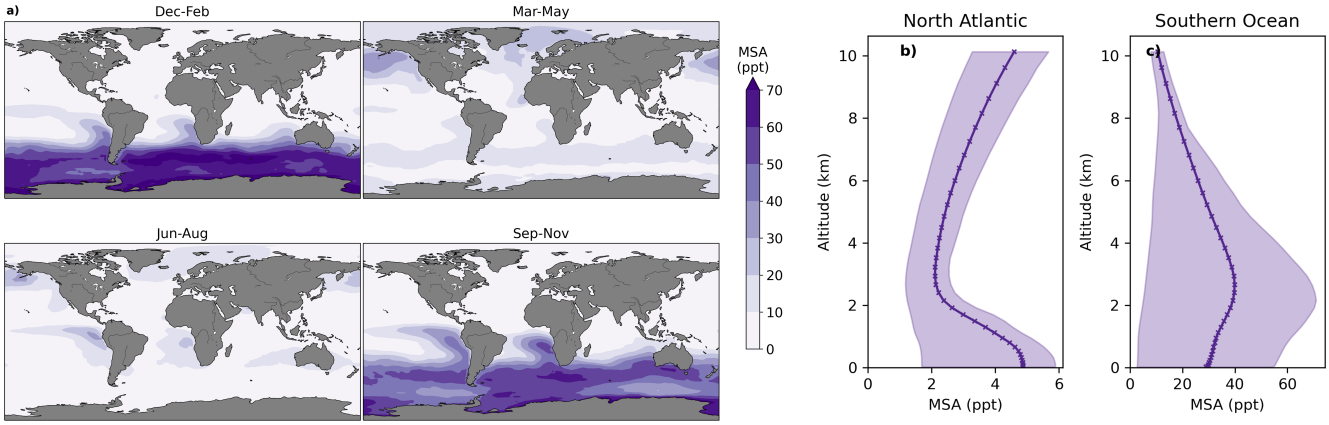

Figure S10: **a)** Global distribution of MSA mixing ratios in the lower troposphere (< 2 km) in CS2-HPMTF. Annual means of the vertical distribution of MSA are shown in the **b)** Central North Atlantic (30-50°E, 20-45°N) and **c)** Southern Ocean (50-70°S). The envelopes represent the interquartile range of the measurements. Note the order of magnitude difference in the MSA concentrations in panels **b)** and **c)**.

S2.1.3 Modelled SO_2 and sulfate

Comparing the three schemes, ST, CS2 and CS2-HPMTF, ST generally has the highest concentrations in SO_2 or sulfate and CS2 the lowest. The difference between the SO_2 mixing ratios in the different schemes is greatest in January/December and lowest in June, both in the Central North Atlantic and the Southern Ocean. This pattern is similar for sulfate concentrations in the Southern Ocean, while sulfate in the North Atlantic is not affected by the different chemical schemes, resulting in similar concentrations for all simulations (due to the large contribution of anthropogenic sources). Additionally, here, sulfate concentration does not follow the same seasonal pattern as SO_2, contrary to the Southern Ocean, where anthropogenic emissions are minimal. In the North Atlantic, the maximum SO_2 and sulfate levels are reached close to the surface (**Figure S11c,d**), tied closely to the fact that the major emissions – shipping and industry – are injected near the surface). SO_2 is depleted quickly in the boundary layer (similar to HPMTF in **Figure 9**), while sulfate concentrations decrease more slowly with height, owing to longer timescales for secondary production from intermediate lifetime DMS oxidation products. In the Southern Ocean however, the maximum SO_2 concentration is only reached at ~2 km in CS2 and ~3 km in CS2-HPMTF and ST. The opposite pattern is observed for the annual mean maximum sulfate concentration by altitude: 1.1 km for ST, 2.4 km for CS-HPMTF and 5.2 km for CS2. This can affect the climate response to DMS emissions because radiative forcing is sensitive to the altitude of aerosols (Krishnamohan et al., 2020). Ranjithkumar et al. (2021) also assessed the ability of UKCA to simulate SO_2 compared with ATom measurements. In their study they used the Lana et al. (2011) emissions and found that reducing the scaling factor to that used by Mulcahy et al. (2018), amongst other changes (cloud pH and aerosol microphysical process changes) gave them the best fit to observations.

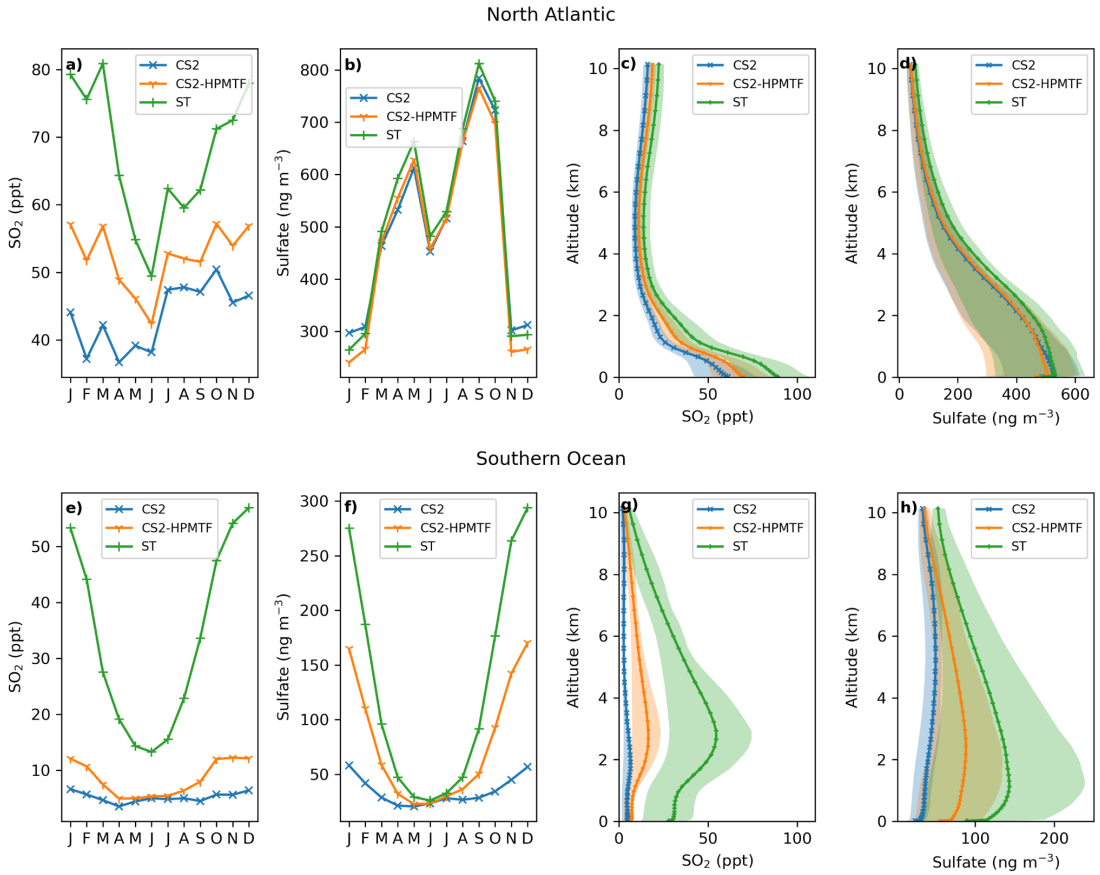

Figure S11: Monthly mean **(a)** SO_2 mixing ratios **(b)** sulfate concentration in the lower troposphere (< 2 km) and the annual mean vertical distribution of **c)** SO_2 and **d)** sulfate concentration in the Central North Atlantic (30-50°E, 20-45°N). The envelopes represent the interquartile range of the measurements. **e) - h)** the equivalent for the Southern Ocean (50-70°S).

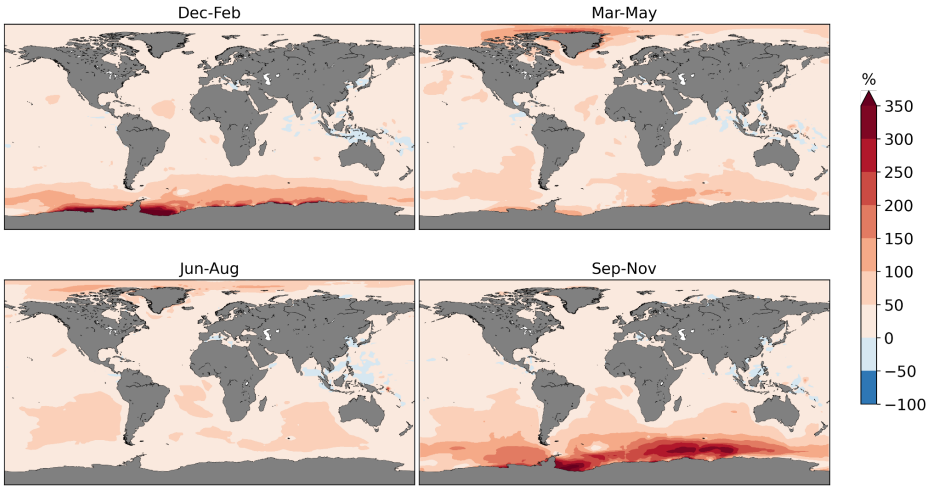

Figure S12: Relative difference in SO_2 mixing ratios in the lower troposphere (< 2 km) between CS2-HPMTF and the base run CS2 (CS2-HPMTF - CS2). Only values above the ocean are shown.

Table S5: Average tropospheric lifetimes of selected species

	CS2	ST	CS2-HPMTF	CS2-HPMTF-FL	CS2-HPMTF-FP
DMS	35.59 h	36.34 h	34.63 h	34.68 h	34.37 h
MTMP	26.61 min	-	0.99 min	0.98 min	0.25 min
DMSO	6.17 h	-	6.15 h	6.16 h	6.09 h
MSA	-	-	6.08 d	6.08 d	6.07 d
MSIA	6.38 h	-	4.81 h	4.81 h	4.74 h
HPMTF	-	-	25.76 h	9.66 h	25.79 h
SO_2					

Table S6: Sulfate in the different aerosol modes by weight.

	Nucleation	Aitken	Accumulation	Coarse
CS2	2.0%	26.2%	69.8%	2.0%
ST	1.7%	27.8%	69.2%	1.4%
CS2-HPMTF	2.1%	26.6%	69.5%	1.8%
CS2-HPMTF-CLD	2.0%	25.5%	70.0%	2.5%

References:

Arsene, C., Barnes, I., and Becker, K. H.: FT-IR product study of the photo-oxidation of dimethyl sulfide: Temperature and O_2 partial pressure dependence, Phys. Chem. Chem. Phys., 1, 5463–5470, https://doi.org/10.1039/A907211J, 1999.

Atkinson, R., Baulch, D. L., Cox, R. A., Crowley, J. N., Hampson, R. F., Hynes, R. G., Jenkin, M. E., Rossi, M. J., and Troe, J.: Evaluated kinetic and photochemical data for atmospheric chemistry: Volume I - gas phase reactions of O_x, HO_x, NO_x and SO_x species, 4, 1461–1738, https://doi.org/10.5194/acp-4-1461-2004, 2004.

Barnes, I., Hjorth, J., and Mihalopoulos, N.: Dimethyl Sulfide and Dimethyl Sulfoxide and Their Oxidation in the Atmosphere, Chem. Rev., 106, 940–975, https://doi.org/10.1021/cr020529+, 2006.

Berndt, T., Scholz, W., Mentler, B., Fischer, L., Hoffmann, E. H., Tilgner, A., Hyttinen, N., Prisle, N. L., Hansel, A., and Herrmann, H.: Fast Peroxy Radical Isomerization and OH Recycling in the Reaction of OH Radicals with Dimethyl Sulfide, J. Phys. Chem. Lett., 10, 6478–6483, https://doi.org/10.1021/acs.jpclett.9b02567, 2019.

Borissenko, D., Kukui, A., Laverdet, G., and Le Bras, G.: Experimental Study of SO2 Formation in the Reactions of CH3SO Radical with NO2 and O3 in Relation with the Atmospheric Oxidation Mechanism of Dimethyl Sulfide, J. Phys. Chem. A, 107, 1155–1161, https://doi.org/10.1021/jp021701g, 2003.

Butkovskaya, N. I. and Barnes, I.: Model Study of the Photooxidation of CH3SO2SCH3 at Atmospheric Pressure: Thermal Decomposition of the CH3SO2 Radical, in: Global Atmospheric Change and its Impact on Regional Air Quality, edited by: Barnes, I., Springer Netherlands, Dordrecht, 147–152, https://doi.org/10.1007/978-94-010-0082-6_22, 2002.

Butkovskaya, N. I. and LeBras, G.: Mechanism of the NO3 + DMS Reaction by Discharge Flow Mass Spectrometry, J. Phys. Chem., 98, 2582–2591, https://doi.org/10.1021/j100061a014, 1994.

Campolongo, F., Saltelli, A., Jensen, N. R., Wilson, J., and Hjorth, J.: The Role of Multiphase Chemistry in the Oxidation of Dimethylsulphide (DMS). A Latitude Dependent Analysis, Journal of Atmospheric Chemistry, 32, 327–356, https://doi.org/10.1023/A:1006154618511, 1999.

Cao, J., Wang, W.L., Gao, L.J. and Fu, F.: Mechanism and thermodynamic properties of CH_3SO_3 decomposition. Acta Physico-Chimica Sinica, 29(6), 1161-1167, https://doi.org/10.3866/PKU.WHXB201304021, 2013.

Chen, H. and Finlayson-Pitts, B. J.: New Particle Formation from Methanesulfonic Acid and Amines/Ammonia as a Function of Temperature, Environ. Sci. Technol., 51, 243–252, https://doi.org/10.1021/acs.est.6b04173, 2017.

Chen, H., Ezell, M. J., Arquero, K. D., Varner, M. E., Dawson, M. L., Gerber, R. B., and Finlayson-Pitts, B. J.: New particle formation and growth from methanesulfonic acid, trimethylamine and water, Phys. Chem. Chem. Phys., 17, 13699–13709, https://doi.org/10.1039/C5CP00838G, 2015.

Chen, J., Berndt, T., Møller, K. H., Lane, J. R., and Kjaergaard, H. G.: Atmospheric Fate of the CH3SOO Radical from the CH3S + O2 Equilibrium, J. Phys. Chem. A, 125, 8933–8941, https://doi.org/10.1021/acs.jpca.1c06900, 2021.

Hoffmann, E. H., Tilgner, A., Schrödner, R., Bräuer, P., Wolke, R., and Herrmann, H.: An advanced modeling study on the impacts and atmospheric implications of multiphase dimethyl sulfide chemistry, PNAS, 113, 11776–11781, https://doi.org/10.1073/pnas.1606320113, 2016.

Hoesly, R. M., Smith, S. J., Feng, L., Klimont, Z., Janssens-Maenhout, G., Pitkanen, T., Seibert, J. J., Vu, L., Andres, R. J., Bolt, R. M., Bond, T. C., Dawidowski, L., Kholod, N., Kurokawa, J., Li, M., Liu, L., Lu, Z., Moura, M. C. P., O'Rourke, P. R., and Zhang, Q.: Historical (1750–2014) anthropogenic emissions of reactive gases and aerosols from the Community Emissions Data System (CEDS), 11, 369–408, https://doi.org/10.5194/gmd-11-369-2018, 2018.

Jenkin, M. E., Young, J. C., and Rickard, A. R.: The MCM v3.3.1 degradation scheme for isoprene, 15, 11433–11459, https://doi.org/10.5194/acp-15-11433-2015, 2015.

Khan, M. A. H., Bannan, T. J., Holland, R., Shallcross, D. E., Archibald, A. T., Matthews, E., Back, A., Allan, J., Coe, H., Artaxo, P., and Percival, C. J.: Impacts of Hydroperoxymethyl Thioformate on the Global Marine Sulfur Budget, ACS Earth Space Chem., 5, 2577–2586, https://doi.org/10.1021/acsearthspacechem.1c00218, 2021.

Krishnamohan, K. S., Bala, G., Cao, L., Duan, L., & Caldeira, K.: The climatic effects of hygroscopic growth of sulfate aerosols in the stratosphere. Earth's Future, 8, e2019EF001326. https://doi-org.ezp.lib.cam.ac.uk/10.1029/2019EF001326, 2020.

Lana, A., Bell, T. G., Simó, R., Vallina, S. M., Ballabrera-Poy, J., Kettle, A. J., Dachs, J., Bopp, L., Saltzman, E. S., Stefels, J., Johnson, J. E., and Liss, P. S.: An updated climatology of surface dimethlysulfide concentrations and emission fluxes in the global ocean, Global Biogeochem. Cy., 25, GB1004 https://doi.org/10.1029/2010GB003850, 2011.

McKee, M. L.: Theoretical study of thet CH3SOO radical, Chemical Physics Letters, 211, 643–648, https://doi.org/10.1016/0009-2614(93)80157-K, 1993.

Mulcahy, J.P., Jones, C., Sellar, A., Johnson, B., Boutle, I.A., Jones, A., Andrews, T., Rumbold, S.T., Mollard, J., Bellouin, N. and Johnson, C.E. Improved aerosol processes and effective radiative forcing in HadGEM3 and UKESM1. Journal of Advances in Modeling Earth Systems, 10(11), pp.2786-2805. 2018.

Novak, G. A., Fite, C. H., Holmes, C. D., Veres, P. R., Neuman, J. A., Faloona, I., Thornton, J. A., Wolfe, G. M., Vermeuel, M. P., Jernigan, C. M., Peischl, J., Ryerson, T. B., Thompson, C. R., Bourgeois, I., Warneke, C., Gkatzelis, G. I., Coggon, M. M., Sekimoto, K., Bui, T. P., Dean-Day, J., Diskin, G. S., DiGangi, J. P., Nowak, J. B., Moore, R. H., Wiggins, E. B., Winstead, E. L., Robinson, C., Thornhill, K. L., Sanchez, K. J., Hall, S. R., Ullmann, K., Dollner, M., Weinzierl, B., Blake, D. R., and Bertram, T. H.: Rapid cloud removal of dimethyl sulfide oxidation products limits SO2 and cloud condensation nuclei production in the marine atmosphere, PNAS, 118, https://doi.org/10.1073/pnas.2110472118, 2021.

Ranjithkumar, A., Gordon, H., Williamson, C., Rollins, A., Pringle, K., Kupc, A., Abraham, N. L., Brock, C., and Carslaw, K.: Constraints on global aerosol number concentration, SO2 and condensation sink in UKESM1 using ATom measurements, Atmos. Chem. Phys., 21, 4979–5014, https://doi.org/10.5194/acp-21-4979-2021, 2021.

Sander, R.: Compilation of Henry's law constants (version 4.0) for water as solvent, Atmos. Chem. Phys., 15, 4399–4981, https://doi.org/10.5194/acp-15-4399-2015, 2015, corrigendum, 2021.

Turnipseed, A. A., Barone, S. B., and Ravishankara, A. R.: Observation of methylthiyl radical addition to oxygen in the gas phase, J. Phys. Chem., 96, 7502–7505, https://doi.org/10.1021/j100198a006, 1992.

Urbanski, S. P., Stickel, R. E., and Wine, P. H.: Mechanistic and Kinetic Study of the Gas-Phase Reaction of Hydroxyl Radical with Dimethyl Sulfoxide, J. Phys. Chem. A, 102, 10522–10529, https://doi.org/10.1021/jp9833911, 1998.

Veres, P. R., Neuman, J. A., Bertram, T. H., Assaf, E., Wolfe, G. M., Williamson, C. J., Weinzierl, B., Tilmes, S., Thompson, C. R., Thames, A. B., Schroder, J. C., Saiz-Lopez, A., Rollins, A. W., Roberts, J. M., Price, D., Peischl, J., Nault, B. A., Møller, K. H., Miller, D. O., Meinardi, S., Li, Q., Lamarque, J.-F., Kupc, A., Kjaergaard, H. G., Kinnison, D., Jimenez, J. L., Jernigan, C. M., Hornbrook, R. S., Hills, A., Dollner, M., Day, D. A., Cuevas, C. A., Campuzano-Jost, P., Burkholder, J., Bui, T. P., Brune, W. H., Brown, S. S., Brock, C. A., Bourgeois, I., Blake, D. R., Apel, E. C., and Ryerson, T. B.: Global airborne sampling reveals a previously unobserved dimethyl sulfide oxidation mechanism in the marine atmosphere, Proc Natl Acad Sci USA, 117, 4505–4510, https://doi.org/10.1073/pnas.1919344117, 2020.

Vermeuel, M. P., Novak, G. A., Jernigan, C. M., and Bertram, T. H.: Diel Profile of Hydroperoxymethyl Thioformate: Evidence for Surface Deposition and Multiphase Chemistry, Environ. Sci. Technol., 54, 12521–12529, https://doi.org/10.1021/acs.est.0c04323, 2020.

von Glasow, R. and Crutzen, P. J.: Model study of multiphase DMS oxidation with a focus on halogens, Atmos. Chem. Phys., 4, 589–608, https://doi.org/10.5194/acp-4-589-2004, 2004.

Wollesen de Jonge, R., Elm, J., Rosati, B., Christiansen, S., Hyttinen, N., Lüdemann, D., Bilde, M., and Roldin, P.: Secondary aerosol formation from dimethyl sulfide – improved mechanistic understanding based on smog chamber experiments and modelling, 21, 9955–9976, https://doi.org/10.5194/acp-21-9955-2021, 2021.

Wu, R., Wang, S., and Wang, L.: New Mechanism for the Atmospheric Oxidation of Dimethyl Sulfide. The Importance of Intramolecular Hydrogen Shift in a CH_3SCH_2OO Radical, J. Phys. Chem. A, 119, 112–117, https://doi.org/10.1021/jp511616j, 2015.

Ye, Q., Goss, M. B., Isaacman-VanWertz, G., Zaytsev, A., Massoli, P., Lim, C., Croteau, P., Canagaratna, M., Knopf, D. A., Keutsch, F. N., Heald, C. L., and Kroll, J. H.: Organic Sulfur Products and Peroxy Radical Isomerization in the OH Oxidation of Dimethyl Sulfide, ACS Earth Space Chem., https://doi.org/10.1021/acsearthspacechem.1c00108, 2021.